ISTITUTO NAZIONALE DI FISICA NUCLEARE

Sezione di Perugia

INFN/AE-95/13
22 Maggio 1995

M.T. Brunetti, A. Codino, C. Grimani, M. Menichelli, M. Miozza, A.S. Stephens:

CHARGED PION ALBEDO INDUCED BY COSMIC ANTIPROTON INTERACTIONS WITH LUNAR SURFACE

SIS-Pubblicazioni
dei Laboratori Nazionali di Frascati

INFN - Istituto Nazionale di Fisica Nucleare
Sezione di Perugia

INFN/AE-95/13
22 Maggio 1995

CHARGED PION ALBEDO INDUCED BY COSMIC ANTIPROTON INTERACTIONS WITH LUNAR SURFACE

M.T. Brunetti[1], A. Codino[1,2], C. Grimani[1], M. Menichelli[1], M. Miozza[1], A.S. Stephens[3]

[1)] INFN–Sezione di Perugia, Via Pascoli, I–06100 Perugia, Italy

[2)] Dipartimento di Fisica Università di Perugia, Via Pascoli, I–06100 Perugia, Italy

[3)] Tata Inst. of Fundamental Res., Homi Bhabha Road, Bombay 400005, India

Abstract

We present a novel approach for the detection of cosmic antiprotons using the lunar surface as a calorimeter. We report the calculations of the energy spectra of single and double charged pion albedo induced by cosmic proton and antiproton interactions with the lunar surface. Properties of such spectra and related fluxes are investigated in order to clarify some important facets of the antiproton detection via charged pion albedo flux from the lunar surface. The method was conceived during the design of the ANTARES detector developed for the quest of cosmic antinuclei in a Moon Orbiting Observatory.

1. Introduction

The detection of galactic cosmic antiprotons arriving at the Earth is hindered by background particles, mainly negative muons, pions and kaons produced in the hadronic showers initiated by primary cosmic rays in the atmosphere. To eliminate these background particles it has long been proposed to operate detectors in space. To date there has been no dedicated experiment that has accomplished the measurement of the cosmic antiproton flux in space. Data gathered so far by balloon-borne experiments are limited to less than about hundred events in the restricted energy range 100 MeV-10 GeV. Space experiments on cosmic antiproton detection have great advantages with respect to balloon-borne experiments. The most evident advantages are the longer data collection times and the absence of atmosphere. In spite of the cleaner environment conditions, space experiments require a lot of efforts. As an example, the transport of passive material of calorimeters and other heavy instruments to satellites or space stations requires many financial and technical resources.

The Moon based experiments constitute another class of space experiments that can avoid some of the drawbacks of balloon-borne and satellite missions. Very clean experimental conditions for antimatter detection are available on the lunar surface and around it. The absence of atmosphere (gas density $\leq 10^{-12}$ g·cm^{-3}) and a negligible magnetic field ($\leq 3 \cdot 10^{-4}$ Gauss) are favorable conditions that give access to the very low energy band of the cosmic radiation.

The possibility to take advantage of the Moon for scientific activities is contemplated in the future explorations of the Solar System, where the Earth satellite represents the first station, followed by Mars, whose exploration is foreseen in the middle of the next century (*Symposium on lunar bases, 1988*).

Cosmic rays hitting the lunar surface produce backward diffused particles (albedo particles) as shown, pictorially, in fig.1. Depending on the distance from the lunar surface, an ideal detector will measure pion, muon, electron and positron fluxes. Our calculation focuses on evaluating the flux of albedo pions induced by antiprotons, and on comparing this signal with the corresponding flux of albedo pions induced by the primary cosmic protons.

This paper was developed during the ANTARES[1] project (*A.Codino et al., 1994*) in which an apparatus was designed to orbit the Moon onto the MORO observatory. This project was proposed to ESA in response to a call for M3 missions in 1992. We conceived an instrumental configuration where the lunar surface plays the role of a calorimeter, hence, drastically reducing the weight of the mission. The active element of the calorimeter is the orbiting apparatus, as foreseen in the original project, or, more conveniently, a Moon based detector (see fig. 1). The lunar soil is made of dust, fine debris and rock fragments and is known as regolith. The chemical composition is mostly made of aluminum and silicon with a depth of several meters.

[1] ANTimatter Assessment RESearch

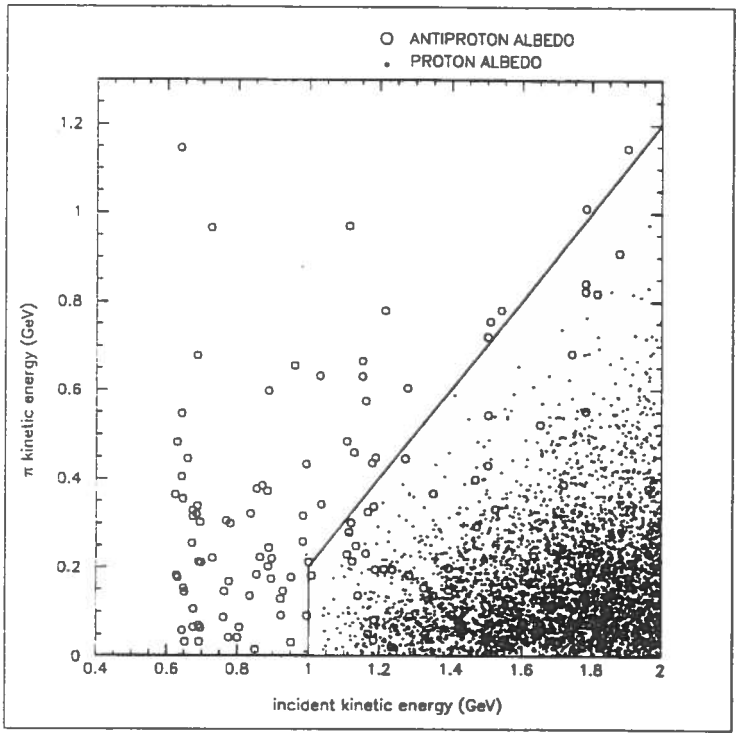

Figure 14: Albedo pion kinetic energy versus incident proton (dots) and antiproton (open circles) kinetic energies for events containing at least two albedo charged pions.

Acknowledgements

We would like to thank Dr. Angioletta Coradini and Prof. Paolo Maffei for useful discussions on the chemical composition and physical parameters of the lunar regolith.

References

G.D.Badhwar and S.A.Stephens - Secondary positrons and electrons in the cosmic radiation, *Proc. 15th International Cosmic Ray Conference*, Plovdiv, Bulgarian Academy of Sciences Vol. **11**, 149 (1977).

M.T.Brunetti et al. - Cosmic antiproton detection by a Moon orbiting observatory, *Nuclear Physics B (Proceeding Supplement Series)* Vol. **43**, 257 (1995).

A.Buffington et al. - *The Astrophysical Journal* **248**, 1179 (1981).

CERN Program Library Manual (1989).

A.Codino et al. - *Il Nuovo Cimento*, **103 B**, N. 3 (1989).

A.Codino et al. - *Astrophysics and Space Science* **220**, 131 (1994).

V. Flaminio et al. - Compilation of cross-sections III: proton and antiproton induced reactions, CERN- HERA 84-01 (1984).

R.L.Golden et al. - *The Astrophysical Journal* **436**, 769 (1994).

E.S.Seo et al. - *The Astrophysical Journal*, **378**, 763 (1991).

S.A.Stephens and G.D.Badhwar - *Astrophysics and Space Science* **76**, 213 (1981).

S.A.Stephens and R.L.Golden - *Space Science Review* **46**, 31 (1987).

S.A.Stephens - *Advances in Space Research* Vol. 9, No **12** (1989).

R.E.Streitmatter et al. - *Advances in Space Research* Vol. 9, No **12** (1988).

Symposium on Lunar Bases and Space Activities of the 21th Century, April 5-7, Houston Texas (1988).

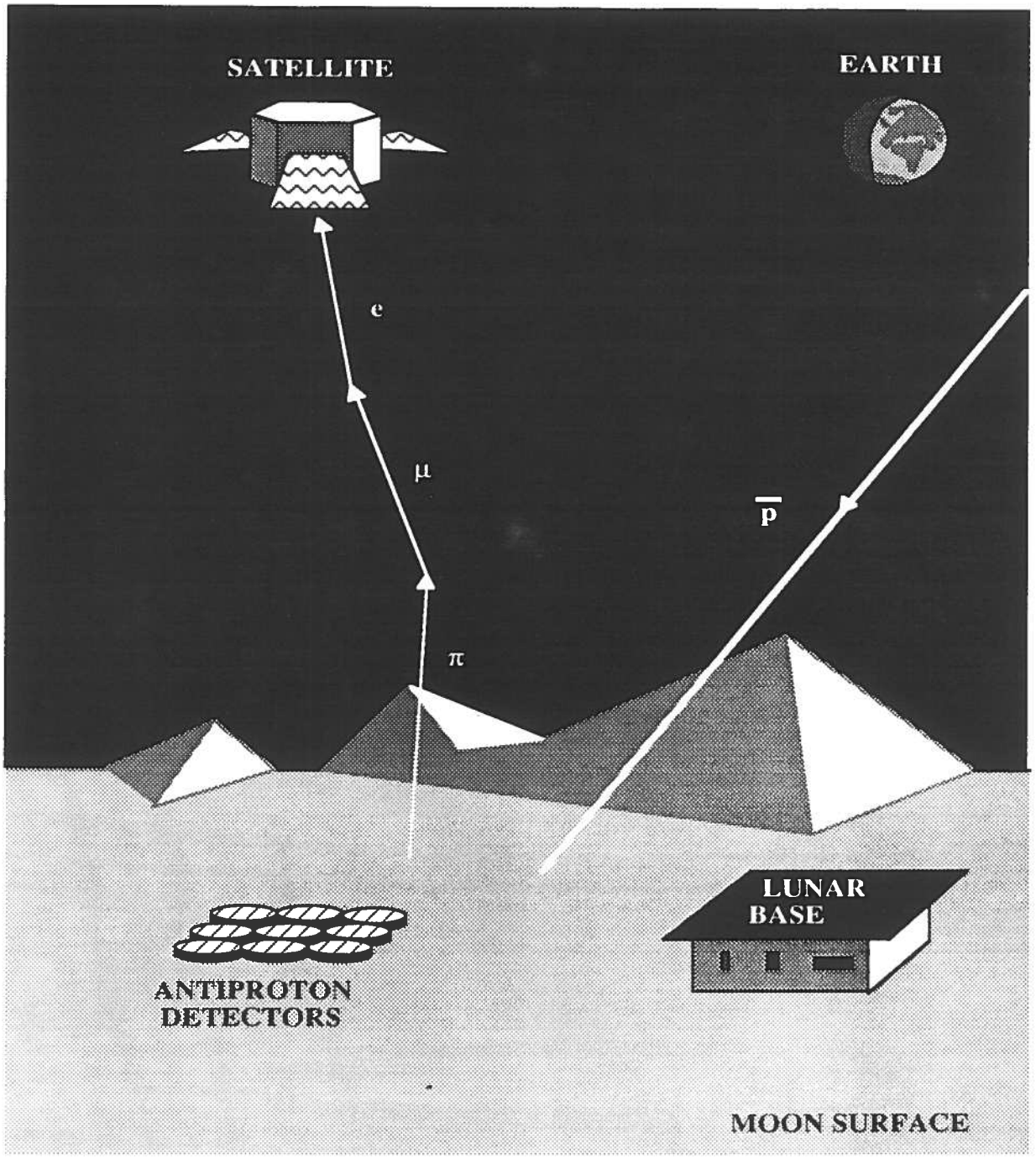

Figure 1: Artistic view of albedo particles from the lunar soil and two instrument configurations capable of detecting charged pions, muons, electrons and positrons. Instruments based on the Moon or housed on orbiting satellites represent two possible experimental configurations for antiproton and antinuclei research. The relative fluxes of albedo particles and of their decay products depend, crucially, on the sampling distance from the Moon surface.

The paper is organized as follows: in section 2 we describe the physical processes generating the pion albedo flux and the related approximations used in the simulation; in section 3 we report the results of the Montecarlo simulation for the flux of charged pions induced by cosmic antiprotons interacting with the lunar surface; in section 4 we report the Montecarlo results for the expected charged pion background induced by cosmic ray protons. We describe also a calculation made to check the simulation results by the analytical method. In section 5 we discuss how the contamination of charged albedo pions generated by cosmic protons may be separated from the corresponding antiproton albedo signal.

2. The physical processes yielding the lunar charged pion albedo

The antiproton detection via the albedo charged pions is based on notable differences in the features of the secondary particle kinematics produced by proton and antiproton interactions with the lunar regolith at low energies.

Experimental data indicate that the cosmic proton flux overwhelms the antiproton flux by a factor at least 10^3 between 100 MeV up to 10 GeV (*S.A.Stephens and R.L.Golden, 1987*). However, the number of backward diffused particles from antiproton-nucleus interactions on the lunar surface, at these energies, is greater than that from proton-nucleus interactions. This is due to the larger kinetic energy carried out by pions emerging from the antiproton-nucleon annihilation stars. The average pion kinetic energy from cosmic antiproton-nucleus interactions turns out to be about 990 MeV, while that of pions from cosmic proton-nucleus collisions about 880 MeV in the energy range 0.6-50 GeV. This energy band includes more than 99% of the cosmic proton flux hitting the lunar surface. As the incident proton energy increases, the charged pion multiplicity increases only logarithmically but the Lorentz boost pushes the secondary particles toward the Moon center. As a consequence, the pion albedo generated by high energy particles decreases to negligible values with respect to that at low energy (see fig. 5 in Section 3 and fig. 7 in Section 4).

In calculating the albedo signal due to protons, we simulate the cosmic proton spectra impinging on the lunar regolith in the kinetic energy range 0.6-50 GeV by a parametrization of the universal cosmic ray power law:

$$J_p = A \cdot E^{-\gamma} \qquad (1)$$

with A and γ depending on the kinetic energy of the incident protons. The flux is parametrized by two curves: the first between 0.6 and 3 GeV with A= 0.110 particles/cm^2·sr·s and γ=1.179,

strongly affected by the solar modulation; and the second for kinetic energy from 3 GeV up to 50 GeV with A=0.355 particles/cm^2·sr·s and γ=2.249. This flux corresponds to a minimum solar activity. It is useful in this calculation to divide the kinetic energy range of the incident cosmic protons and antiprotons into three regions: low energy E<3 GeV, medium energy, between 3 GeV and 10 GeV and high energy E>10 GeV. The convenience of this partition is related to the parametrization used in the calculation.
The lower kinetic energy limit of about 600 MeV for the incident cosmic proton spectrum is dictated by the negligible cross sections for the reactions p p —> p n π^+, p n —> n n π^+ and p p —> d π^+ at threshold energies. Note that the threshold energy in the reaction p p —> d π^+ is 287 MeV.

The following approximations are used in the present calculation:

(I) charged pions decaying into muons are neglected. This assumption represents a good approximation since the average distance between the pion production point in the regolith and the lunar surface is few centimeters. Pions with kinetic energy of 140 MeV have a mean path of 15.6 m before decaying into muons.

(II) Experimental data for the parametrization of the inclusive invariant cross section for pion production ($E\cdot d^3\sigma/dp^3$), that we have used in the analytical calculation, are available only for proton-proton reactions. The corresponding parametrization for antiproton-proton interactions is unavailable. Accordingly, reliable analytical calculations for antiproton-proton interactions producing albedo have not been accomplished.

(III) The inclusive charged pion production cross section ($E\cdot d^3\sigma/dp^3$) is available from experimental data for laboratory proton energy greater than about 1.5 GeV (*G.D.Badhwar and S.A.Stephens, 1977*). At lower energies, relevant for our calculations, this cross section is not available. In these circumstances we made, in the lower energy range 600 MeV-1.5 GeV, a crude extrapolation of the cross section ($E\cdot d^3\sigma/dp^3$) used at higher energies.

(IV) The Fermi motion of the target nucleons in nuclei is neglected.

(V) The Coulomb scattering in the lunar regolith for protons, antiprotons and pions is neglected.

(VI) The lunar regolith is assumed to be made of aluminum. In table I we report some simple parameters pertaining antiproton and pion propagation in aluminum.

TABLE I

Ionization energy losses and range for charged pions versus energy in the lunar regolith. Inelastic interaction length λ_I, annihilation length λ_a and range for antiprotons in the energy interval 20 MeV-1 GeV in the lunar regolith.

PIONS			ANTIPROTONS		
Kinetic Energy (MeV)	dE/dx (MeV/cm)	π range in Al (cm)	$\bar{p}$ range in Al (cm)	λ_I in Al * (cm)	λ_a in Al* (cm)
20	12.5	0.9	0.2	28	7
30	9.5	1.6	0.4	31	9
40	8.0	2.7	0.7	31	10
50	7.1	4.1	0.9	32	11
60	6.5	5.2	1.4	32	13
70	6.0	6.7	1.9	33	14
80	5.7	8.5	2.3	33	15
90	5.5	9.6	2.8	34	17
100	5.3	11.5	3.5	34	17
200	4.6	30	11	38	20
300	4.5	50	22	39	23
400	4.5	72	35	40	27
500	4.5	93	50	40	28
600	4.6	114	60	41	30
700	4.7	130	80	42	31
800	4.7	152	100	43	32
900	4.8	175	120	43	34
1000	4.8	190	140	44	37

* Calculated

3. Charged pion albedo induced by cosmic antiprotons

The flux of charged albedo pions induced by cosmic antiprotons on the lunar surface has been calculated by the Montecarlo method. The nuclear cross sections for proton-antiproton interactions in the kinetic energy interval 0.6-50 GeV are parametrized following a CERN experimental compilation (*V.Flaminio et al., 1984*) and have been utilized in previous calculations (*A.Codino et al., 1989*).

Relevant geometrical parameters of the calculation are shown in fig. 2. The incoming cosmic antiproton hits the lunar surface with an angle θ_P with respect to the zenith direction. Then, it propagates into the regolith and undergoes ionization energy losses before interacting with a nucleus at depth x_D. Pions produced in the annihilation stars or in the inelastic interaction vertex depart with an angle θ with respect to the zenith. Depending on θ, bound in the range $0\text{-}\pi/2$, pions will escape the regolith or propagate deeper in it. The low kinetic energy pions will never reach the surface stopping in the lunar soil. We used the Bethe-Block formula to calculate the mean ionization energy losses in the regolith. The contribution to the pion albedo from interaction vertexes deeper than 200 cm is neglected in our calculation (see also table I) because of the small fraction of pions produced at such depths. The number of these pions is further reduced by ionization energy losses.

The incident antiproton energy spectrum employed in this calculation is reported in fig.3. It is derived from a fit of available experimental data on antiproton-to-proton ratio using the proton flux measured in 1987 at solar minimum (*E.S.Seo et al., 1991*) in three kinetic energy intervals between 0.6 and 50 GeV. These experimental data do not significantly differ from those reported by S. A. Stephens (*S.A.Stephens, 1989*). More sophisticated parametrization of the incident antiproton spectra would be unrealistic and unreliable due to the large error bars in the available experimental data and to the conflicting measurements in the antiproton fluxes between 100 MeV and 800 MeV (*A.Buffington et al., 1981; R.E.Streitmatter et al., 1988*).

In order to simulate the charged pion production, we generate antiproton event samples, as large as 10^7, hitting the lunar soil with isotropic arrival directions. The inclusive charged pion energy spectrum generated in the regolith by antiprotons in the energy range 0-4 GeV, at any depth, is shown in figure 4. Figure 5 shows the charged albedo pion flux as a function of the incident antiproton kinetic energy. Ionization energy losses suffered by pions from the production point backward to the lunar surface are included in the spectrum of fig. 5. As expected, the pion flux decreases at increasing energies of the incident antiprotons. The shape of the curve comes from the convolution of the incident antiproton spectrum (shown in fig. 3) and the pion albedo curve, which decreases at increasing energies due to the Lorentz boost. The charged pion albedo spectrum, evaluated at the lunar surface, is shown in fig. 6 and represents a fraction of that reported in fig. 4. These pions have, in fact, enough kinetic energy and the right trajectory to escape the lunar surface. The mean value of the spectrum in fig. 6 is around 590 MeV, while the peak position is at 100 MeV.

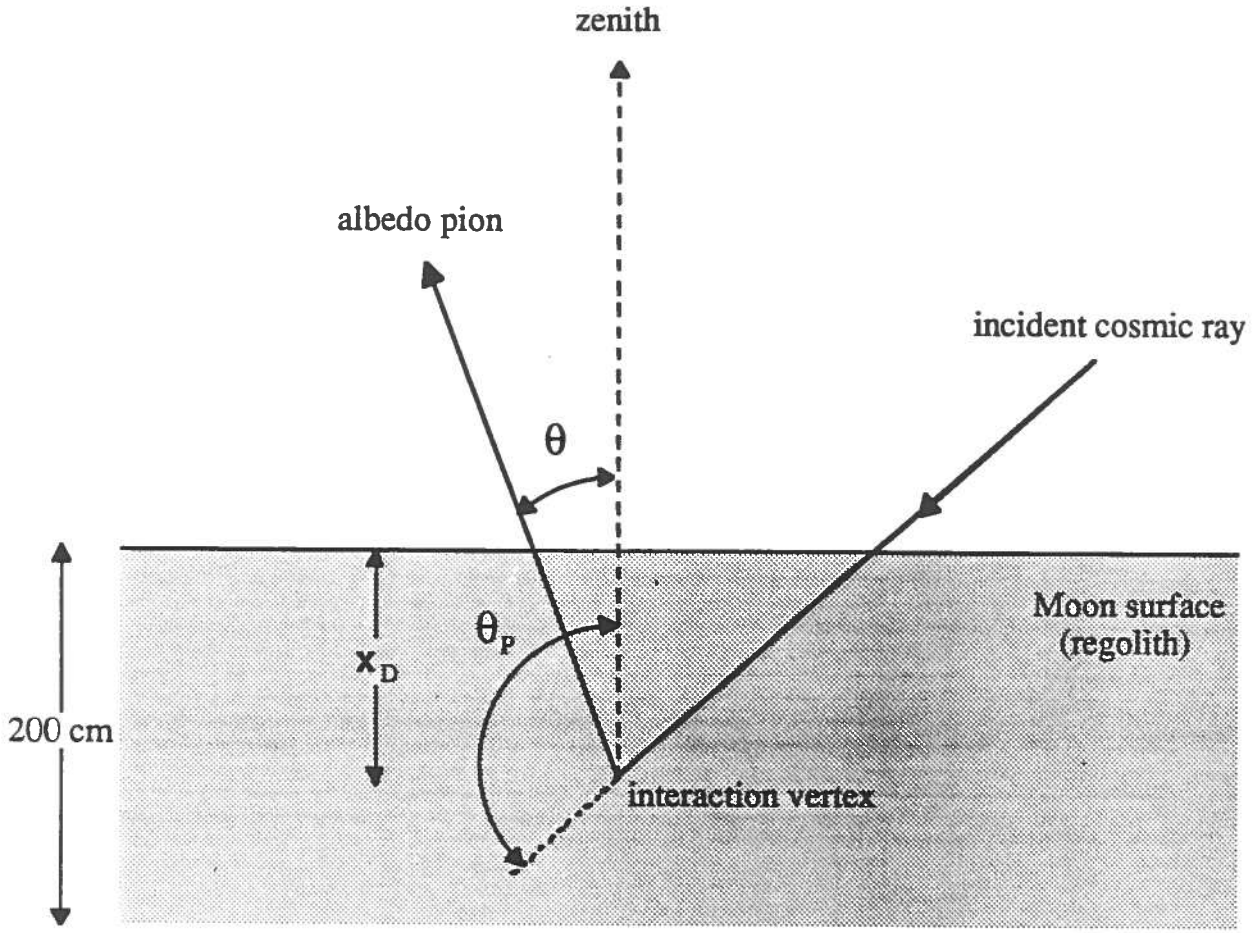

x_D = interaction depth in the regolith

θ = charged pion scattering angle

θ_P = antiproton incident angle

Figure 2: Incident angle θ_P of the incoming cosmic protons and antiprotons defined in the range $90° \leq \theta_P \leq 180°$. At interaction depths, x_D, greater than 200 cm there is no contribution to the pion albedo because of the ionization energy losses.

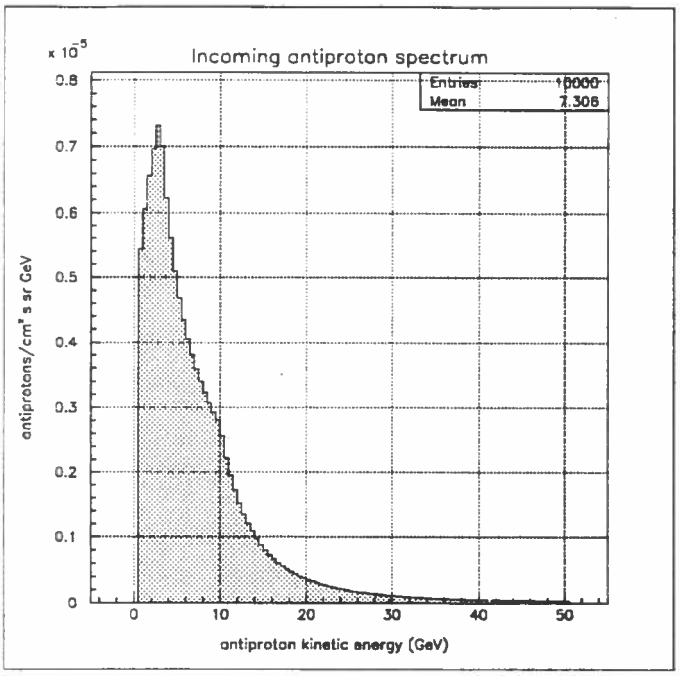

Figure 3: Energy spectrum of 10000 cosmic antiprotons hitting the lunar soil at minimum solar modulation used in the simulation code. The mean kinetic energy is about 7.3 GeV and the peak energy is at about 3 GeV.

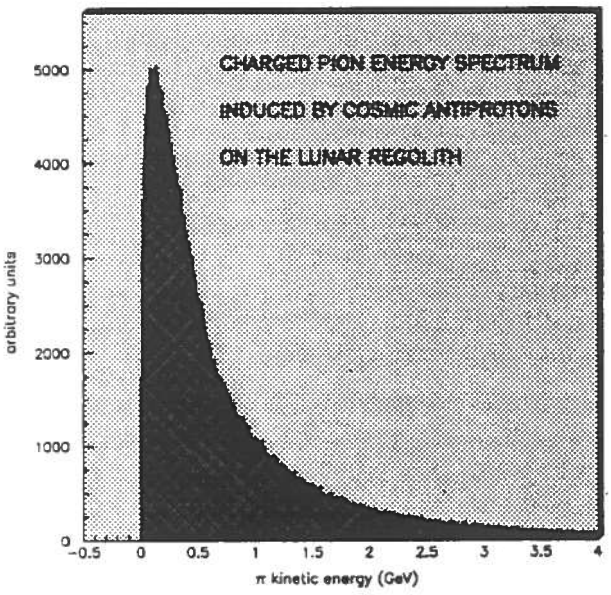

Figure 4: Inclusive charged pion spectrum induced by antiproton interactions in the lunar regolith. The average pion kinetic energy is about 990 MeV and the peak position around 140 MeV.

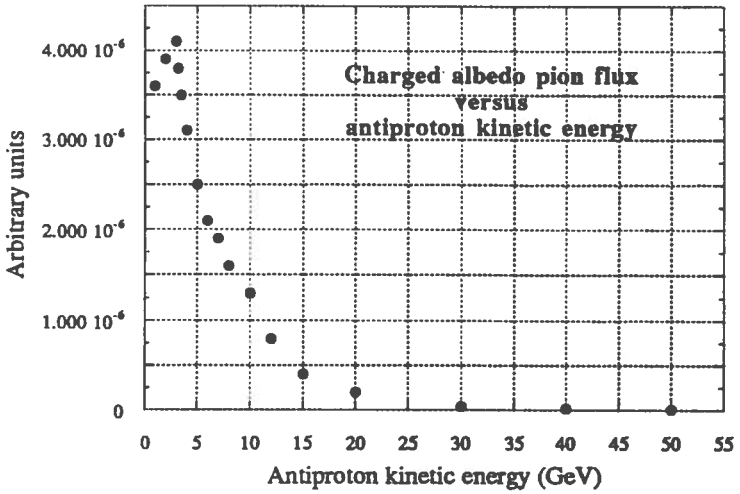

Figure 5: Charged pion albedo flux from the lunar surface versus the antiproton kinetic energy in the range 600 MeV-50 GeV. Note that only 2.3% of the incident antiprotons have energies below 600 MeV.

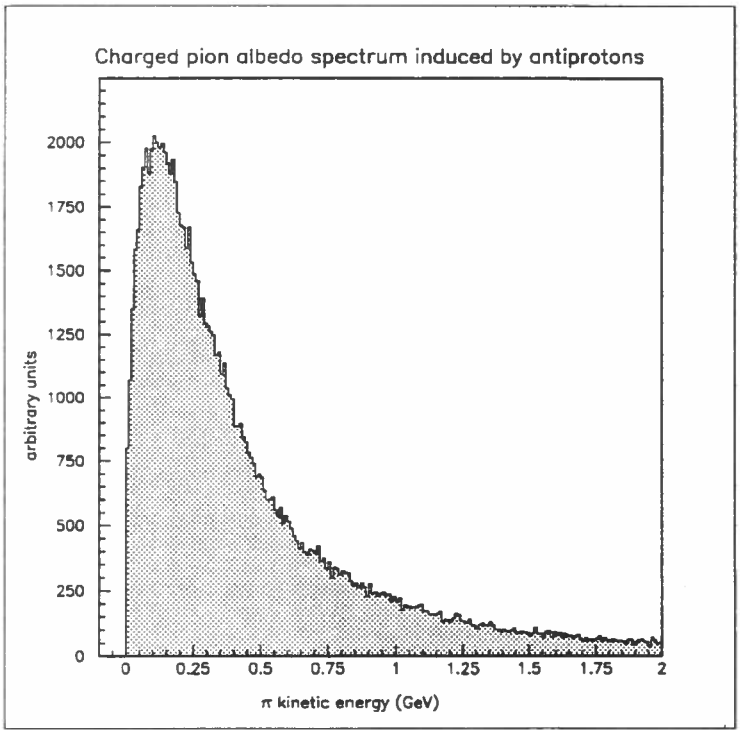

Figure 6: Energy spectrum of the antiproton induced pion albedo escaping the lunar surface. The mean pion kinetic energy is 590 MeV.

4. Charged pion albedo induced by cosmic protons

In this section we report the charged pion albedo induced by cosmic protons calculated with both Montecarlo and analytical method.

The pion albedo energy spectrum induced by proton interactions, was calculated by the simulation code LEASA (LEASA is for Low Energy Antiproton Simulation Algorithms) described elsewhere (*A.Codino et al., 1989*). The program has been checked in balloon-borne experiments dedicated to the antiproton and electron flux measurement (*R.L.Golden et al., 1994*). The LEASA code simulates the exclusive reaction channels for proton-proton and proton-neutron interactions in the range 0.6-50 GeV. Particle momenta after the interaction are calculated by the phase space algorithm given by the CERN libraries (*CERN Program Library Manual, 1989*). Results are shown in figs. 7 and 8. In particular, in fig. 7 is reported the flux of albedo charged pions escaping the lunar surface versus the kinetic energy of the incident protons, similar to the corresponding curve for antiprotons in fig. 5. As for antiprotons, the flux decreases at increasing energies and its value at 10 GeV is one order of magnitude less than that at 1 GeV. The albedo pion energy spectrum induced by cosmic protons is shown in fig.8. The average kinetic energy is 596 MeV and is peaked at 70 MeV. About 70% of the albedo pions have a kinetic energy lower than 1 GeV. This signal represents the background flux to be identified and detected from the Moon surface by a suitable detector.

In order to cross-check the Montecarlo results, we have also performed an analytical calculation of the proton induced background. Previous analytical estimates of the charged pion albedo generated by cosmic protons hitting the Moon surface have been published (*M.T.Brunetti et al., 1995*). As mentioned in section 2, this check is possible only for proton interactions, since the parametrization of the inclusive pion cross section for antiprotons is unavailable.

In order to calculate the pion albedo background induced by cosmic protons, some useful parameters employed in the calculation need to be defined. They are the incident proton angle θ_p, the interaction depth x_D and the scattering angle θ defined as the direction of the incident proton and the zenith (see fig. 2).

The quantity $q(E,x_D)$ in particles/s·cm^3·GeV in the following equation (2) gives the number of positive charged pions with energy E escaping in the backward direction, along the zenith, per second per unit area at the depth x_D deep in the lunar surface (*S.A.Stephens and G.D.Badhwar, 1981*):

$$q(E,x_D) = 2\pi\rho_{Al}\left(\frac{\lambda_p}{\lambda_{Moon}\, m_p}\right)\int_E^{\infty} dE' \int_{\frac{\pi}{2}}^{\pi} d\theta\; p \sin\theta \left(E\frac{d^3\sigma}{dp^3}\right) J_p(E',x_D,\theta) \qquad (2)$$

where ρ_{Al} is the aluminum density, λ_p is the interaction length of the proton in hydrogen, λ_{Moon} the proton interaction length in the Moon regolith and m_p is the proton mass. The double integration is made over the incoming proton energy E' and on the scattering angle θ. The integrand contains the perpendicular component of the charged pion momentum $p \cdot \sin\theta$ and the integration takes into account only those pions escaping along the zenith direction.

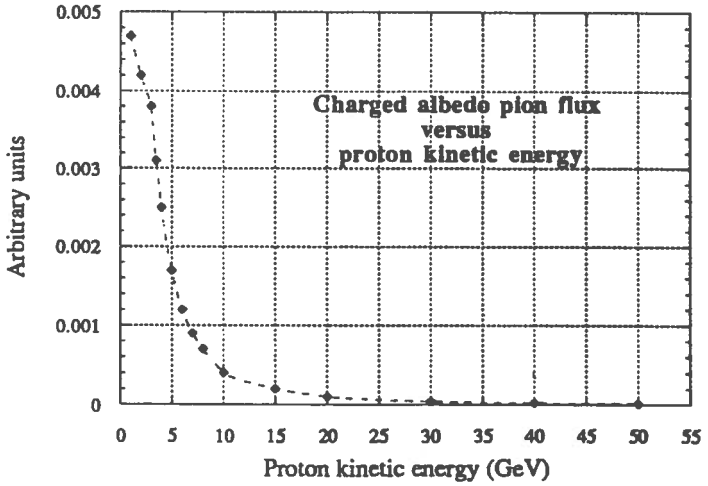

Figure 7: Flux of albedo charged pions escaping the lunar surface versus the proton kinetic energy.

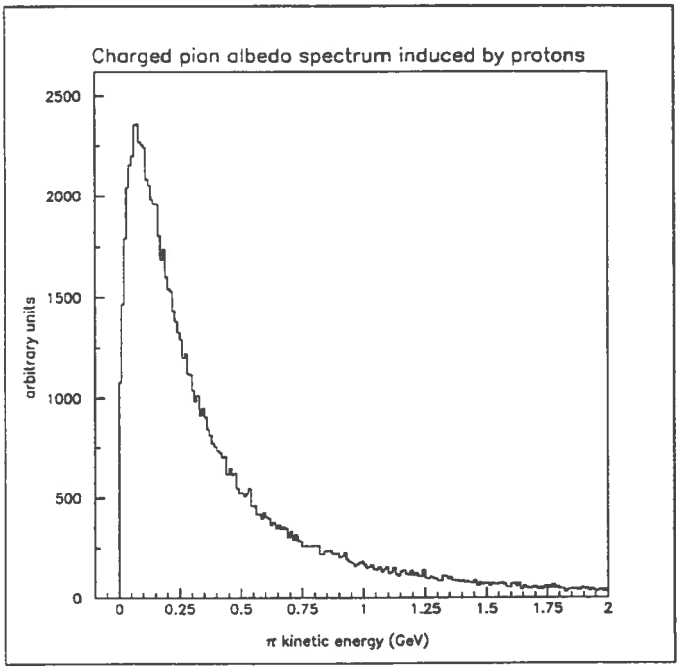

Figure 8: Inclusive single charged pion albedo spectrum induced by cosmic protons generated by Montecarlo simulation.

The term ($E\,d^3\sigma/dp^3$) is the inclusive invariant cross section for charged pion production in the proton-proton collision and $J_p(E',x_D,\theta)$ is the incident flux for protons with energy E'and scattering angle θ as defined in fig. 2. In this analytical calculation the albedo flux is evaluated along the zenith direction, which implies $\theta=\theta_p$.

The inclusive invariant cross section of the reaction including all charged pion production processes

$$p + p \longrightarrow \pi^+ + \text{anything}$$

has been interpolated by the following expressions (*G.D.Badhwar and S.A.Stephens, 1977*):

$$E\frac{d^3\sigma}{dp^3} = \frac{fA}{\left(1+4\frac{m_p^2}{s}\right)^r}\,\tilde{Z}^q \exp\left[-Bp_\perp/\left(1+4\frac{m_p^2}{s}\right)\right] \qquad (3)$$

$$E\frac{d^3\sigma}{dp^3} = \frac{fA}{\left(1+4\frac{m_p^2}{s}\right)^r}\left(1-4\frac{m_p^2}{s}\right)^{2q-k}\tilde{Z}^{k-q} \exp\left[-Bp_\perp/\left(1+4\frac{m_p^2}{s}\right)\right] \qquad (4)$$

Equation (3) holds for $0 \le \tilde{Z} \le \left(1-\frac{4m^2}{s}\right)$ and equation (4) holds for $\tilde{Z} > \left(1-\frac{4m^2}{s}\right)$, where:

$f= 1+ 3.2\cdot10^4\cdot E^{-10.5} + 47.5\cdot E^{-2.15}$, k=3, A=153, r=1 and B=5.55 for the positive charged pions; f=1, k=5, A=127, B=5.3 and r=3 for the negative charged pions.
The variable $\tilde{Z}$ is related to the Feynmann variable $\tilde{x}$ by the following relationship:

$$\tilde{Z} = (1-\tilde{x}) - \left[1-\left(1+\frac{4m_p^2}{s}\right)^{\frac{1}{2}}\right]\frac{p_\perp}{p^*}$$

where

$$\tilde{x} \approx \sqrt{x_{//}^{*2} + \frac{4}{s}(m_\pi^2 + p_\perp^2)} \quad \text{with} \quad x_{//}^* = \frac{p_{//}^*}{p_{max}^*}$$

where $p^*_{//}$ and p^*_{max} are, respectively, the parallel component and the maximum value of the pion momentum in the center-of-mass system of the colliding particles.

The exponent q can be expressed by :

$$q = \frac{(C_1 + C_2\, p_\perp + C_3\, p_\perp^2)}{\sqrt{1 + 4\frac{m_p^2}{s}}}$$

with C_1=5.3667, C_2=-3.5 and C_3=0.8334 for π^+ and C_1=7.0334, C_2=-4.5 and C_3=1.667 for π^-. Figure 9 shows the positive pion energy spectra produced at increasing depths by protons hitting the Moon surface. The lunar regolith has been divided in layers of 1 cm thickness and the corresponding albedo pion fluxes have been calculated. The resulting spectra reported in fig. 9 show peaks centered between 20 and 30 MeV. The mean value decreases as the production depth increases, as a consequence of the lower incident kinetic energy available and of the flux attenuation.

The fluxes from all layers are summed up to the lunar surface and corrected for ionization energy losses. The results are shown in fig. 10.

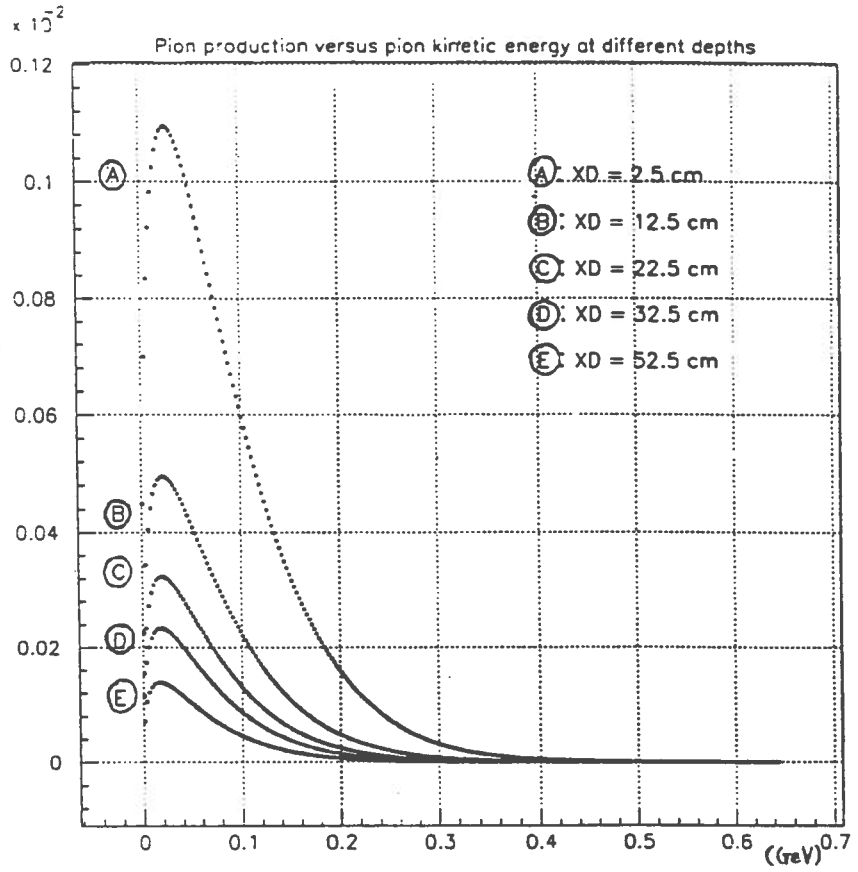

Figure 9: Analytical energy spectra of positive pion albedo induced by cosmic proton interactions in the lunar regolith, at various depths. The kinetic energy interval of the cosmic incident protons is between 0.6 and 10 GeV. Note that the maximum of the π^+ spectra is weakly sensitive to the depth and is placed around 20 MeV. Note also that at the depth of 12.5 cm in the lunar regolith the flux is halved.

We verified that the segmentation in layers of 1 cm thickness does not bias the flux calculation. The peak position is shifted to ≈30 MeV with respect to that at 20 MeV (fig.9). The greater is the depth, the greater the threshold in the albedo pion kinetic energy to escape the Moon. Note that the total charged pion albedo flux ($1.2 \cdot 10^{-4}$ particles$\cdot$cm$^{-2}\cdot$s^{-1}) escaping from the lunar surface along the zenith is reduced by a factor ≈50 with respect to that produced inside the regolith because of the ionization energy losses. The fluxes calculated by the analytical method should be integrated in a convenient solid angle around the zenith direction and, consequently, cannot be directly compared to the Montecarlo results.

The angular dependence of the charged pion albedo flux emanating from the Moon has been calculated with the Montecarlo method and is shown in fig. 11 for both protons and antiprotons. When the incident proton or antiproton angle varies from 5° to 80° the resulting pion albedo flux increases by a factor of about 25. The shapes of antiproton and proton curves are slightly different.

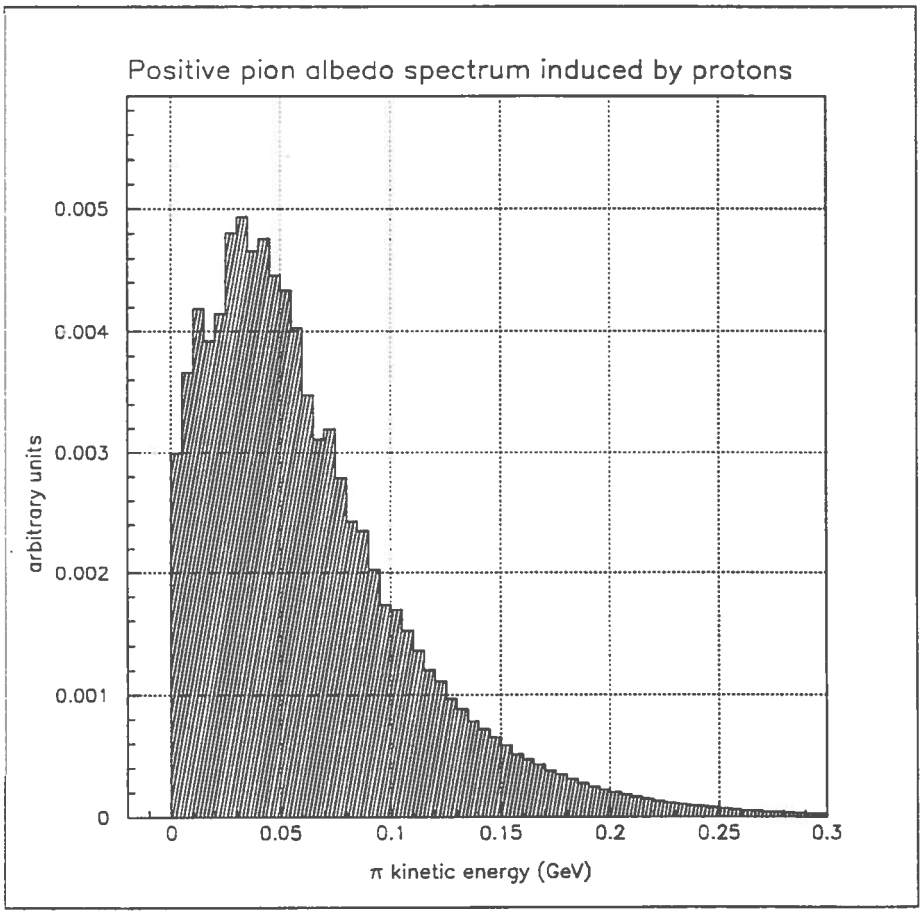

Figure 10: Analytical energy spectra for cosmic proton induced positive charged pion albedo escaping the lunar regolith.

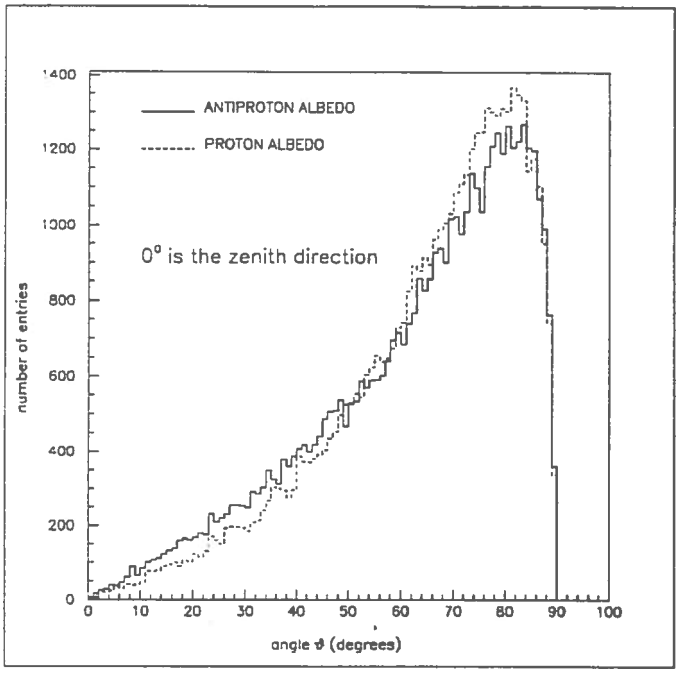

Figure 11: Angular distribution of charged albedo pions generated by a sample of cosmic protons and antiprotons impinging on the lunar regolith.

5. Cosmic antiproton signal and proton background via albedo pions

In this section we describe and discuss some criteria to identify what fraction of the charged pion albedo flux is composed of particles induced by cosmic antiprotons.

The charged pion albedo flux induced by cosmic protons turns out to be $1.409 \cdot 10^{-1}$ pions/cm^2·s, while that induced by antiprotons $1.93 \cdot 10^{-4}$ pions/cm^2·s. Note that in the present calculation the antiproton-to-proton flux ratio in the lunar regolith is $2.5 \cdot 10^{-4}$ in the energy interval 600 MeV-50 GeV.

Let us imagine that an ideal detector is located on the Moon surface, registering all charged albedo pions induced by cosmic rays, including antiprotons. Below we assume a detection efficiency of 1. The efficiency of the antiproton detection measured by means of the charged pion albedo and registered by this ideal detector is 52.0% for antiprotons and 9.59% for protons. Thus, there is a difference of about a factor 5 in the detection efficiency of protons and antiprotons by means of pion albedo.

However, the inclusive charged pion albedo energy spectra of protons and antiprotons do not display significant differences. Note that the small, unfavorable antiproton-to-proton flux ratio would further obscure the antiproton signature.

In order to enhance the antiproton signal over the proton induced background from the previous evaluation, we required at least two charged pions for each interaction in the inclusive pion albedo spectrum. Since this criterion is very selective, the antiproton detection efficiency reduces to 25.3% and that of protons to 1.33%. In this circumstance the charged albedo pion fluxes is $1.955 \cdot 10^{-2}$ pions/cm^2·s for protons and $9.4 \cdot 10^{-5}$ pions/cm^2·s for antiprotons. The ideal detector, shaped by a square of 1 m^2 lying on the Moon surface would register about 320606 antiprotons per day, according to the incident antiproton flux discussed in section 3.

Figures 12 and 13 show energy spectra for the charged pion albedo generated by protons and antiprotons with two or more albedo pions per event. The average kinetic energy and peak energy values of the two spectra do not differ significantly. The average kinetic energy of two or more charged pion albedo events induced by antiprotons is 630 MeV, while that of single pion albedo events, shown in fig. 6, is 615 MeV.

Despite the similarity of the reported spectra in figs. 12 and 13, the separation of proton induced events may be obtained by the bidimensional plot shown in fig. 14, which gives the kinetic energies of albedo pions versus those of the incident protons and antiprotons. Clearly, the method assumes the measurement of the incident kinetic energy of protons and antiprotons and that of albedo pions. It turns out from fig. 14 that only protons with kinetic energy greater than 1 GeV contribute to the two pion albedo events. The two segments in fig. 14 defined by the coordinate pairs (1;0)GeV-(1;0.2)GeV for the first segment and (1;0.2)GeV-(2;1.2)GeV for the second segment split the plane into two zones. In the upper portion of the plane the pion contamination induced by cosmic protons to the antiproton induced events is less than 4%. Regardless of the specific instrument designed to measure the antiproton flux, this low level contamination may be used for consistency checks in any future experiment.

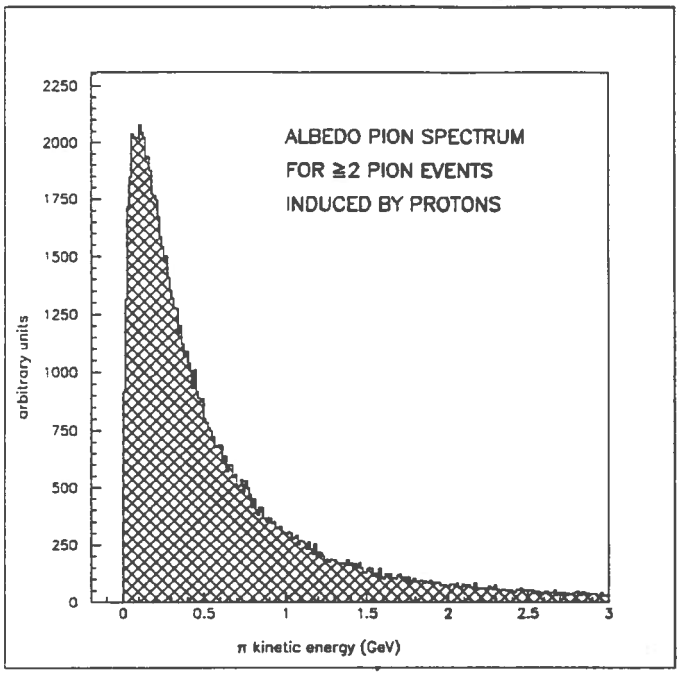

Figure 12: Energy spectra of the proton induced charged pion albedo for two or more albedo pion events.

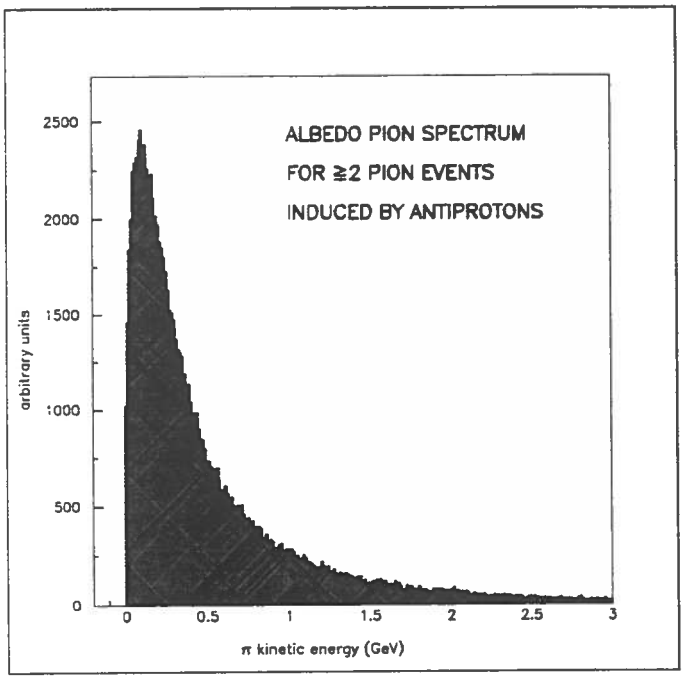

Figure 13: Energy spectra of the antiproton induced charged pion albedo for two or more albedo pion events.